



Journal of Advanced Research in Fluid Mechanics and Thermal Sciences

Journal homepage:
https://semarakilmu.com.my/journals/index.php/fluid_mechanics_thermal_sciences/index
ISSN: 2289-7879



Performance Evaluation of Photovoltaic Thermal using MgO Nanofluid

Sam Yih Herng¹, Mohd Afzanizam Mohd Rosli^{1,*}, Nurfahana Salimen¹, Safarudin Ghazali Herawan², Faridah Hussain³

¹ Faculty of Mechanical Engineering, Universiti Teknikal Malaysia Melaka, Hang Tuah Jaya, 76100 Durian Tunggal, Melaka, Malaysia

² Industrial Engineering Department, Faculty of Engineering, Bina Nusantara University, Jakarta, 11430 Indonesia

³ SIRIM Standards Technology Sdn. Bhd., Seksyen 15, 40200 Shah Alam, Selangor, Malaysia

ARTICLE INFO

Article history:

Received 28 June 2023

Received in revised form 4 September 2023

Accepted 13 September 2023

Available online 29 September 2023

Keywords:

Electrical Efficiency; MgO Nanofluid;
Overall Efficiency; Surfactant; Thermal
Efficiency

ABSTRACT

This study investigated the performance and efficiency of a photovoltaic thermal (PV/T) system utilizing a metal-based nanofluid, specifically MgO nanofluid. This research proposes MgO as nanoparticle to mix with base fluid because it demonstrated to have superior features with the highest thermal conductivity and lowest viscosity among the metal oxide. The nanofluid offered improved thermophysical properties that enhanced the PV/T system performance. The study focused on formulating a stable nanofluid, determining its thermophysical properties, and analysing the overall system performance. 0.2wt% MgO nanofluid were successfully developed and demonstrated excellent stability over a 14-day period by using a two-step method which 20 minutes of homogenization at 1000rpm and 30 minutes of ultrasonication. Tests were conducted to determine the thermal conductivity and viscosity of the nanofluid at various concentrations and temperatures. Results showed that increasing the concentration and temperature enhanced thermal conductivity, while viscosity increased with concentration but decreased with temperature. The thermal and electrical efficiencies of the PV/T system at various irradiances (200W/m², 500W/m² and 800W/m²), and flow rates (10L/h, 20L/h, 30L/h) were examined, calculated and compared between water and the MgO nanofluid as working fluids. At 10L/h, it was observed that nanofluid had the highest 74% of thermal efficiency increment compared to the water at 500W/m² followed by 71% at 200W/m² and 55% at 800W/m². Also, Nanofluid demonstrated a 5% increase in electrical efficiency at 200W/m², 2.1% increase at 500W/m², and 1.9% increase at 800W/m² compared to water. The nanofluid exhibited superior thermal and electrical efficiency compared to water, indicating its potential for improving system performance hence, surpassing the performance of a standalone PV system.

1. Introduction

The energy crisis and greenhouse gas emissions are currently the two major issues plaguing the entire globe. The primary component of greenhouse gases, CO₂, had a sharp increase between 2011 and 2021, which led to an increase in Earth's temperature. CO₂ emission grew from 390 parts per million in 2011 to 414.47 parts per million in 2021 [1,2]. As a result of increasing energy demand and

* Corresponding author.

E-mail address: afzanizam@utem.edu.my

<https://doi.org/10.37934/arfmts.109.2.184209>

environmental concern, developing renewable energy technologies has received strong and sustained interest for a few decades. Among the renewable energy sources available, solar energy is a renewable energy which doesn't release a harmful natural gases or hazardous products unlike with other energy sources such as fossil fuels and nuclear energy [3]. Solar power facilities tend to reduce the environmental impacts from the combustion used in fossil fuel power generation, such as impacts from greenhouse gases and other air pollution emissions [4].

Photovoltaic cells (PV) are made of semiconductor materials which produce electricity by converting sunlight radiation which stimulates electrons [5]. As only a fraction of the solar spectrum is utilized in this process to excite electrons to create electron-hole pairs, the photovoltaic cells have limited electrical efficiency. Photovoltaic cells mainly absorb the solar spectrum between 700 nm and 1100 nm [5]. Shorter or longer wavelengths are not collected but converted to heat that can reduce cell efficiency or, to some extent, cause damage. The PV panel temperature is considered a critical issue when forecasting energy production. When solar irradiance falls on the PV cell, it cannot fully convert the solar energy into electric energy. A fraction of the solar radiation is transformed to heat energy that raises the PV cell temperature. PV efficiency decreases around 0.5% for every degree of temperature increase of the panel [5,6]. Only a part of solar energy is converted into electrical energy while the other part of energy is converted into heat energy. The conversion of efficiency is from 12% to 18% [7]. Produced heat accumulated on the surface of the PV panels increases its working temperature hence decreases the electrical efficiency of the PV panels. Therefore, to improve the efficiency of the PV systems, thermal collectors are combined with and installed beneath the PV panels. The combination of these systems is known as photovoltaic thermal (PV/T) system consisting of a heat transfer fluid inside a tube or container with a solid surface that absorbs heat [8].

In contrast, PV/T system is one of the ways to solve the problem of heat accumulated on the PV panel by absorbing the heat through the working fluid and at the same time produce electricity. PV/T system is combination of PV panel and solar collector where the PV panel produces electricity while solar collector act as a solar absorber to absorb the excessive heat around PV panel and transfer it for another usage [9,10]. However, the use of air and water as a working fluid in the PV/T had limited the efficiency of PV/T system in terms of electrical and thermal due to its low thermal conductivity of air and water which are 0.00623W/mK and 0.598W/mK respectively [11]. So, nanofluids which had great potential to enhance heat absorption as well as transportation capacity were introduced by most of the researchers [1,12]. Since their inception, a lot of research has been done with respect to application of nanofluid as heat absorbing and transport medium in heating and cooling systems. A Nanofluid is a fluid in which nano-sized particles suspended in the base fluid form a colloidal solution of nanoparticles in the base fluid have been found to possess enhanced thermophysical properties such as thermal conductivity, thermal diffusivity, viscosity, and convective heat transfer coefficients compared to those of base fluids like oil or water [13,14]. The nanofluid which has high thermal conductivity is a crucial point to enhance the performance of the PV/T system in terms of electrical and thermal efficiency.

Al-Ghezi *et al.*, [15] conducted an experimental study using CuO nanofluid in PV/T systems. Different weight ratios (0.5%, 1.0%, 1.5%, and 2%) of CuO nanoparticles in water were prepared. The results showed that the electrical efficiencies increased by 3.3%, 12.97%, 20.3%, and 29.92% for the corresponding CuO weight ratios. Similarly, the thermal efficiencies increased by 12.65%, 26.9%, 37%, and 61.08% with increasing CuO concentration. The overall efficiencies of the PV/T system also improved, reaching 15.95%, 38.87%, 57.3%, and 91% for the respective CuO weight concentrations. In an experimental study by Sardarabadi *et al.*, [16] the use of SiO₂ nanofluid in a PV/T system was investigated. The results showed a maximum electrical efficiency of 13.31% for a SiO₂ nanofluid with a mass fraction of 3%. The equivalent thermal efficiency was significantly higher for the SiO₂ nanofluid

compared to the conventional system, with values of 69.2% and 72.1% for mass fractions of 1% and 3%, respectively, compared to 28.9% for the conventional system. The average overall efficiencies for the system were 49.8% and 52.4% for the SiO₂ nanofluid with mass fractions of 1% and 3%, respectively, while the reference system had an average overall efficiency of only 11%. So, Table 1 and Table 2 summarize some of the recent works in this field which focus on nanofluid metal based on PV/T systems.

Table 1
 Summarise of the previous research

Study Type	Nanoparticle Type	Concentration & Base Fluid	PV Panel Specifications	Optimum Flow rate	Thermal Efficiency Enhancement	Electrical Efficiency Enhancement	Total Overall Efficiency	Ref
Exp	Al ₂ O ₃ CuO SiC	0.5, 1, 2, 3, 4 vol% H ₂ O	110W APM-P 110-12	-	Al ₂ O ₃ - 1.96% CuO - 3.42% SiC - 4.8%	-	-	Al-Waeli <i>et al.</i> , [11]
Exp	CuO	0.5, 1, 1.5, 2 wt% H ₂ O	APM-P 110-12	-	CuO 0.5wt% - 12.65% CuO 1wt% - 26.9% CuO 1.5wt% - 37% CuO 2wt% - 61.08%	CuO 0.5wt% - 3.3% CuO 1wt% - 12.97% CuO 1.5wt% - 20.3% CuO 2wt% - 29.92%	CuO 0.5wt% - 15.95% CuO 1wt% - 38.87% CuO 1.5wt% - 57.3% CuO 2wt% - 91%	Al-Ghezi <i>et al.</i> , [15]
Exp	Fe ₃ O ₄ SiO ₂ Fe ₃ O ₄ /SiO ₂	3 wt% Deionized water	30W mono-crystalline silicon	20 L/min 30 L/min 40 L/min	At 20 L/min: Fe ₃ O ₄ - 38% SiO ₂ - 40% Fe ₃ O ₄ /SiO ₂ - 42%	At 20 L/min Fe ₃ O ₄ - 12.5% SiO ₂ - 13.15% Fe ₃ O ₄ /SiO ₂ - 13.85%	Fe ₃ O ₄ /SiO ₂ : 20 L/min: 57% 30 L/min: 62% 40 L/min: 67%	Khan <i>et al.</i> , [17]
Exp	Al ₂ O ₃	0.3 vol% H ₂ O	Mono-crystalline	0.2 L/s	Al ₂ O ₃ - 34.4%	Al ₂ O ₃ - 12.1%	-	Hussien <i>et al.</i> , [18]
Exp	Fe ₃ O ₄	1, 3 wt% Distilled water	40W mono-crystalline silicon	-	1100W/m ² Fe ₃ O ₄ 1 wt% - 65.96% Fe ₃ O ₄ 3 wt% - 68.42%	1100W/m ² Fe ₃ O ₄ 1 wt% - 7.23% 600W/m ² Fe ₃ O ₄ 3 wt% - 7.14%	Fe ₃ O ₄ 1 wt% - 76%	Ghadiri <i>et al.</i> , [19]
Exp & Num	SiC TiO ₂ SiO ₂	1 wt% H ₂ O	110W polycrystalline silicon	0.05- 0.167 kg/s	SiC - 87% TiO ₂ - 86% SiO ₂ - 80%	500W/m ² SiC - 16.5% TiO ₂ - 15.5% SiO ₂ - 14.4%	-	Hasan <i>et al.</i> , [20]

Exp = Experiment, Num = Numerical Analysis, Ref = Reference

Table 2

Summarise of the previous research using MgO nanofluid

Study Type	Nanoparticle Type	Concentration & Base Fluid	PV Panel Specifications	Optimum Flow rate	Thermal Efficiency Enhancement	Electrical Efficiency Enhancement	Total Overall Efficiency	Ref
Exp	MgO	0.08 vol% EG/Distilled water (1:1 vol%)	Solar Collector Flat plate	-	At 2.5 L/min MgO 0.2% - 15.57% MgO 0.14 % - 13.2% MgO 0.08% - 9.3%	-	-	Choudhary <i>et al.</i> , [21]
Exp	MgO	0.25, 0.5, 0.75, 1, 1.25, 1.5 vol% Double distilled water	Solar Collector Flat plate	0.5, 1, 1.5, 2, 2.5L/min	At 1.5 L/min mass flow rate, MgO 0.75 vol% enhanced 9.34% compared with water Enhancement lesser for 1.5 and above vol% due to agglomeration"			Verma <i>et al.</i> , [22]
Exp	MgO	0.02, 0.06%, 0.1% Deionized water	25W PV Module	8 L/h	PV/T with a 2mm thick liquid film: 47.2% PV/T with a 4mm thick liquid film: 32%	PV/T with a 2mm thick liquid film: 14.7% PV/T with a 4mm thick liquid film: 14%	PV/T with a 2mm thick liquid film: 61.9% PV/T with a 4mm thick liquid film: 46%	Cui and Zhu [23]

Exp = Experiment, Num = Numerical Analysis, Ref = Reference

2. Methodology

2.1 Experiment Setup and Configuration

The experimental setup for PV analysis consists of two NSD-15W polycrystalline silicon photovoltaic modules, each housing 12 solar cells. The PV module's specification is summarized in Table 3. Among these modules, one of the modules is equipped with a collector, allowing it to function as a PV/T unit, while the other module does not have a collector and serves as a standard photovoltaic module. The PV/T comprises a copper serpentine pipe with an inner diameter of 10mm and a thickness of 1mm, securely welded to a copper plate to enhance heat transfer capabilities at the back of the PV as shown in Figure 1.

To simulate the required solar irradiation for evaluating the photovoltaic modules, a solar simulator features 12 halogen lamps, each with a power rating of 500W was employed. The lamps are arranged in a 3 x 4 matrix to ensure uniform distribution of irradiance as shown in Figure 2. A voltage regulator controller facilitates adjustments to the lamp intensity, allowing from a range of 100 W/m² to 1200 W/m². Apogee's pyranometer is used to measure the incident irradiation by the solar simulator by positioning parallel to the photovoltaic surfaces. The modules' temperature is recorded by using PicoLog TC-08 and while the electrical performances were assessed by using an Array 3721A 400Watt Programmable DC Electronic Load.

Table 3
Specification of PV Module

Solar module type	NSD-15W Polycrystalline Silicon
Peak power	15W
Max. power voltage	6V
Max. power current	2.5A
Open circuit voltage	7.2V
Short circuit current	2.75A
Tolerance	±5%
Operating temperature	-20°C - 90°C

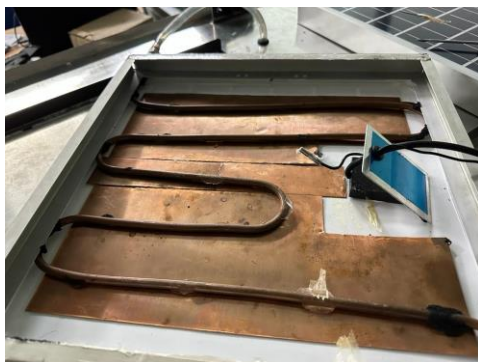


Fig. 1. Copper serpentine tube welded on the copper plate at the back of the PV/T module



Fig. 2. Arrangement of the halogen lamps

In terms of experimental parameters, various solar irradiance levels were tested, ranging from 200W/m², 600W/m² and 800W/m². Additionally, the mass flow rate of the working fluid was adjusted using a water flow meter DK800-6, with increments set at 10L/h, 20L/h, and 30L/h. The working fluids, which were water and nanofluid utilized were stored in a tank and circulated around the PV/T via a circulation pump brand Verderflex Rapide R3. The whole experiment system schematic diagram is shown in Figure 3.

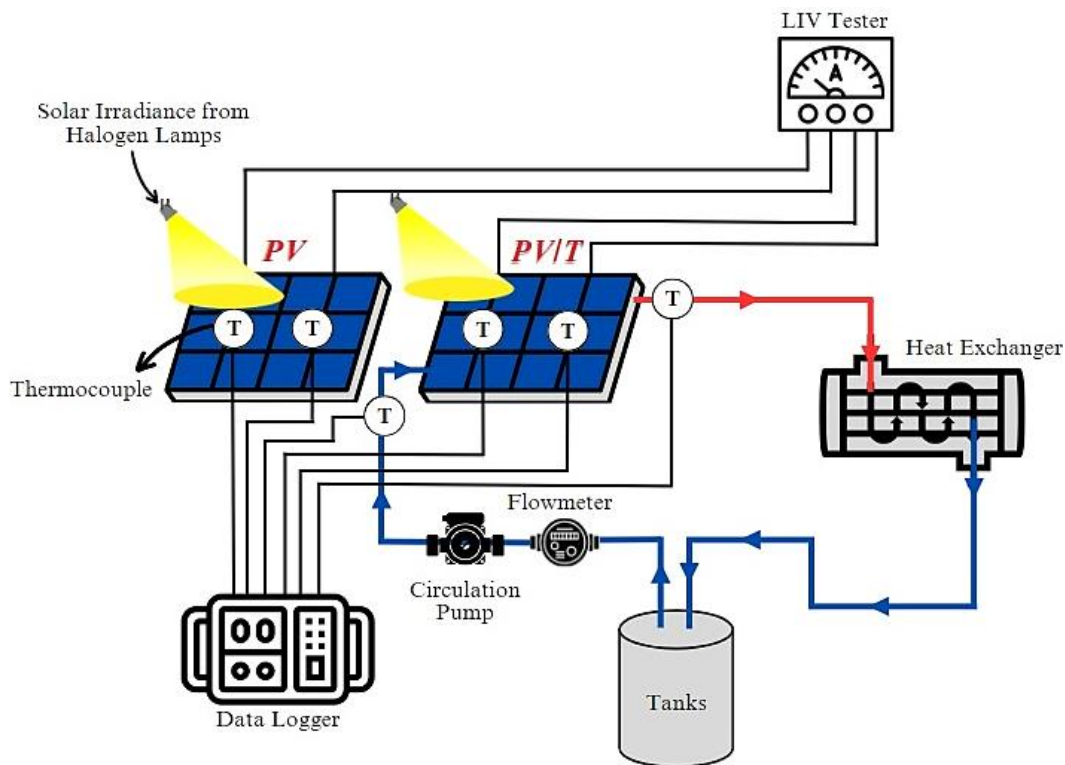


Fig. 3. Schematic diagram of the experiment setup

2.2 Characterization of Nanoparticles

To determine the characteristics of the nanoparticles MgO, FESEM and XRD were employed. FESEM analysis was performed using device Hitachi SU 500. The FESEM images captured with this instrument were utilized to examine the morphology, assess agglomeration, and measure the particle size of the MgO nanoparticles in the magnification of 25kX and 100kX. Meanwhile, the XRD analysis conducted on PANalytical XPert PRO operating at Cu K radiation ($\lambda = 1.5406 \text{ \AA}$) in the 2θ range of 10-80 degrees, with a scanning step of 0.05 degrees and a scan speed of 5 degrees per minute as referred to Bdewi *et al.*, [24]. XRD analysis was utilized to validate the purchased MgO nanoparticles, assess their purity, and determine particle size by identifying crystal structures and analyzing diffraction peaks. As referred to Salman *et al.*, [25] the particles size was determined by using Debye-Scherrer equation as shown in Eq. (1):

$$D = \frac{K\lambda}{(\beta \cos \theta)} \quad (1)$$

where β represents the full width at half maximum height (FWHM) of the diffraction peak at an angle (in radians), θ is the angle of Bragg diffraction, λ is the XRD wavelength (in nm), and K is a dimensionless shape factor.

2.3 Synthesis of Nanofluids

A two-stage method was employed for the synthesis of nanofluid in the present study. Different concentrations of nanofluid (0.2, 0.4, 0.6, 0.8, 1.0 wt%) were mixed to determine the most stable formulation. A two-stage method involving homogenization 20 min at 1000rpm using homogenizer HG-15D and sonication using Easy Elmasonic device for 30min ensuring a well-mixed and stable

nanofluid for further experimental analysis. The required quantity of nanoparticles needed for a particular volume concentration of 100ml nanofluid was calculated using the following Eq. (2) [26-28]:

$$\phi\% = \frac{(m_p/\rho_p)}{(m_p/\rho_p)+(m_f/\rho_f)} \times 100\% \quad (2)$$

where ϕ represents the weight concentration of the nanofluids, m_p, m_f are the mass of nanoparticles and base fluid, ρ_p, ρ_f are the density of the nanoparticles and the base fluid. Table 4 and Table 5 showed the details and properties of the nanoparticles and base fluid included the CAS number of distilled water and MgO nanoparticles which represent the series number of the items. While Table 6 presents corresponding weights of nanoparticles required to achieve specific concentrations of the nanofluid.

Table 4

Details of the material used in the present study

Name	Category	Function	CAS Number
Distilled water	Dispersed phase	Base fluid	7732-18-5
MgO nanoparticles	Dispersion medium	Nanoparticle	1309-48-4

Table 5

Nanoparticle and base fluid properties

Particle	ρ_p (kg/m ³)	k_p (W/m ² °C)	Purity (%)	d_p (nm)	Colour
MgO	3580	48	99.8	40-60	White
Base fluid	ρ_f (kg/m ³)	k_f (W/m ² °C)	CP _f (J/kg°C)	μ_f (nm)	Colour
Distilled Water	997.1	0.608	4184	0.000957	Colourless

Table 6

Weight of the MgO for different weight concentrations

MgO concentration (wt%)	Mass MgO (g)
0.2	0.7195
0.4	1.4419
0.6	2.1673
0.8	2.8955
1	3.6267

2.4 Stability Test (Observation Method)

After preparation, the nanofluid samples were carefully transferred into individual containers, ensuring proper labeling and identification. The containers were securely sealed to prevent evaporation or contamination and stored under controlled temperature conditions to maintain consistency. As referred to Ali *et al.*, [29], visual observation or sedimentation and centrifugation methods were then conducted to assess the presence and extent of sedimentation within the nanofluid samples. The samples were examined for visible settling or sedimentation at the container's bottom. The nanofluids are considered to be stable when the particle size of bouncy particles keeps constant while unstable if there were sedimentation occurred at the bottom of the bottle. Additionally, the clarity and homogeneity of the nanofluid were evaluated. Photographs of the nanofluid samples were captured within 24 hours after preparation, as well as 7 and 14 days after synthesis, to observe the stability of the nanofluids over time.

2.5 Thermophysical Properties Test

2.5.1 Density

The density of MgO nanofluids were estimated by using theoretical models. One widely accepted model for calculating the density of nanofluids is the Pak and Cho mode. As referred to Ali *et al.*, [26] the Pak and Cho model is represented by Eq. (3):

$$\rho_{nf} = (1 - \phi)\rho_{bf} + \phi\rho_{np} \quad (3)$$

where the ρ_{nf} represent of density of nanofluid, ϕ is the weight concentration, ρ_{np} and ρ_{bf} is density of the nanoparticles and base fluid respectively.

2.5.2 Specific heat capacity

Based on mixture law specific heat of nanofluids can be expressed as a function of the volume concentration and density of individual element [26]. The nanofluids specific heat capacity can be calculated using following Eq. (4):

$$C_{p,nf} = \frac{(1-\phi)(\rho C_p)_{bf} + \phi(\rho C_p)_{np}}{\rho_{nf}} \quad (4)$$

where the $C_{p,nf}$ represent of specific heat of nanofluid, C_{bf} and C_{np} is specific heat capacity of the nanoparticles and base fluid respectively, ϕ is the weight concentration and ρ_{np} and ρ_{bf} is density of the nanoparticles and base fluid respectively.

2.5.3 Thermal conductivity

Tempos Thermal Analyzer with KS-3 sensor was utilized to measure the thermal conductivity of the nanofluids. KS-3 sensor was selected for its capability to measure thermal conductivities ranging from 0.02-2.0 W/m·K. Before initiating the test, the Tempos Thermal Analyzer was calibrated following the manufacturer's guidelines. Once the calibration was complete, the KS-3 sensor was connected to the Tempos Thermal Analyzer. The sensor was securely placed within the sample cell of the analyzer to establish proper contact with the nanofluid specimen to ensure accurate and reliable thermal conductivity measurements throughout the testing process. The measurement process was repeated multiple times to ensure the accuracy and consistency of the results [30].

In order to obtain the thermal conductivity results of the nanofluid at various temperatures, the nanofluid sample was allowed to reach thermal equilibrium with the desired test temperature. This was achieved by utilizing a hotplate stirrer. The sample was carefully placed on the hotplate and stirred gently to ensure uniform temperature distribution. The heating process was carefully monitored until the nanofluid reached the desired test temperature. Once the sample reached thermal equilibrium, the thermal conductivity test was performed by repeating the step above.

2.5.4 Viscosity

The viscosity of the nanofluids was determined using an IKA ROTAVISC lo-vi viscometer equipped with a VOL-SP-6.7 and VOL-C-RTD-1 chamber. The viscometer was calibrated according to the manufacturer's instructions to ensure precise and reliable measurements. The VOL-SP-6.7 spindle

and VOL-C-RTD-1 chamber were securely attached to the viscometer. Prior to each measurement, the chamber was carefully cleaned and dried to prevent any potential contamination. During the measurement, the VOL-SP-6.7 spindle was immersed into the nanofluid sample, and the rotational speed was set to 150 rpm, covering the range of nanofluid viscosities. The viscometer was then initiated, and three readings were taken for each concentration to ensure accuracy. To avoid any cross-contamination, the spindle was cleaned and dried between measurements.

To assess the viscosity of the nanofluid at different temperatures, the sample was allowed to equilibrate with the desired test temperature. This was achieved using a hotplate stirrer. The sample was placed on the hotplate and gently stirred to ensure uniform temperature distribution. Once the targeted temperature, the viscosity test was performed as described above.

2.6 Solar Simulator Setup, Validation and Testing

2.6.1 Uniformity test

Uniformity test of a solar simulator is conducted to assess the evenness of the irradiance distribution from the halogen lamps across the target area since the solar irradiance is manually controlled by the voltage regulator. A paper with a grid (12cm x 10cm) was positioned beneath the halogen lamps as shown in Figure 4. The pyranometer was utilized to measure irradiance at each point of the grid and the results were recorded. 200W/m², 500W/m² and 800W/m² of irradiances were tested for its uniformity and ensure the results within the range of plus minus 10% of the set irradiance.

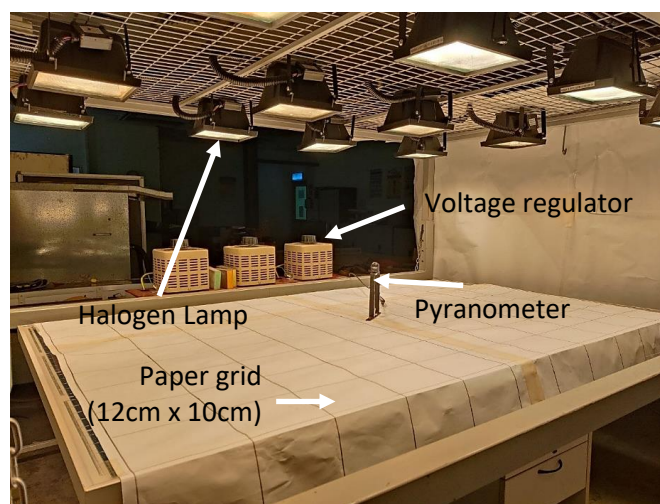


Fig. 4. Set up of uniformity test

2.6.2 Spectral characteristics test

The aim to conduct the spectral characteristics test was to observe and identify the differences between spectral wavelength of halogen lamps and natural sun light. The spectral wavelength test is conducted to analyze the spectral distribution of the light emitted by the halogen lamps of the solar simulator and the natural sunlight. The test involved collecting the halogen light wavelength within the range of 200W/m² to 800 W/m², as well as the real sun's wavelength at regular intervals from 8am, 10am, 12pm, 2pm and 4pm by using spectrometer.

2.6.3 Temporal test

The objective of this test was to observe the cooling behavior of the modules and determine the time it took for them to reach the initial temperature. The temporal test for a PV and PV/T module involves monitoring and observing the temperature of the module as it gradually drops to the ambient temperature or normalized temperature. The temporal test for the PV and PV/T modules involved subjecting them to an 800W/m² irradiance level under a solar simulator for a duration of 5 minutes. After the exposure, the PV and PV/T were isolated from any additional heat sources and left it to cool down naturally. The measurements were recorded over time until the modules reached a stable temperature close to the initial temperature.

2.7 Measurement of Efficiency

2.7.1 Thermal efficiency

To calculate the thermal efficiency of the PV/T system for different kind of working fluids, the Eq. (5) is used as referred to the previous study by Al-Waeli *et al.*, [11]:

$$\eta_{th} = \frac{(\dot{m} \cdot c_p \cdot (T_o - T_i))}{(I \cdot A_c)} \times 100 \quad (5)$$

where the \dot{m} represents the mass flow rate in L/s, c_p represents the specific heat capacity, T_o and T_i represents the temperature outlet and inlet of the PV/T system, I represents the solar intensity and A_c is the collector area.

2.7.2 Electrical efficiency

To calculate the thermal efficiency of the PV/T system in different kind of working fluids, as referred to Al-Waeli *et al.*, [11] the Eq. (6) was employed:

$$\eta_e = \frac{P_{max}}{(I \cdot A_c)} \times 100 \quad (6)$$

where the P_{max} is the maximum power produced by the PV/T, I is the solar intensity and A_c is the collector area.

2.7.3 Overall efficiency

As referred to Al-Waeli *et al.*, [11], the overall efficiency performance of the PV/T system is calculated by Eq. (7) below:

$$\eta_{total} = \eta_e + \eta_{th} \quad (7)$$

where the η_e and η_{th} obtained from the Eq. (5) and Eq. (6) respectively.

3. Results

3.1 Solar Simulator Setup, Validation and Testing

3.1.1 Uniformity test

Based on the results at Table 7, 8 and 9, it was found that the solar simulator exhibited a high degree of uniformity in the irradiance distribution for all three levels of irradiances $200\text{W}/\text{m}^2$, $500\text{W}/\text{m}^2$ and $800\text{W}/\text{m}^2$. The measured intensities at different points on the grid were within the acceptable range of plus or minus 10% of the set irradiance. This meant that the solar simulator provides consistent and uniform irradiance conditions for subsequent experiments.

Table 7

Result uniformity test for $200\text{W}/\text{m}^2$

192	198	194	188	200	213	199
219	217	190	182	196	206	197
213	216	203	203	209	212	206
211	218	211	220	220	218	203
210	213	217	220	215	217	204
220	216	219	203	214	222	207
196	209	210	200	220	210	215
180	193	197	210	219	211	218
183	188	184	199	219	219	215

Table 8

Result uniformity test for $500\text{W}/\text{m}^2$

480	495	485	470	500	533	498
548	543	475	455	490	515	493
533	540	508	508	523	530	515
528	545	528	548	550	545	508
503	533	543	550	538	550	510
550	540	550	508	535	550	518
490	523	525	500	550	525	538
450	483	493	525	548	528	545
458	470	460	498	548	548	538

Table 9

Result uniformity test for $800\text{W}/\text{m}^2$

720	743	728	730	750	799	746
821	814	713	683	735	773	739
799	810	761	761	784	795	773
791	818	791	825	818	818	761
754	799	814	800	806	825	765
825	810	825	761	803	833	776
735	784	788	750	825	788	806
740	724	739	788	821	791	818
734	762	720	746	821	821	806

3.1.2 Spectral characteristics test

From Figure 5, the graph showed that there is a significant overlap in the wavelength range between sunlight and the halogen lamps. This indicates that the halogen lamps are capable of emitting light within the desired spectral range for solar simulation. Although the wavelength ranges

overlap, it was observed that there was an approximate 18% deviation between the values obtained for sunlight and halogen lamps by calculated the area under the graph. From Figure 6, the graph shows that while the solar irradiance increases, the pattern in spectral radiation intensity also increases, but the wavelength pattern maintains constant. These results showed that as the radiation intensity increases, the energy emitted by the light source also intensifies. The constant wavelength indicates that the light emitted by the source remains consistent or constant in terms of its frequency and color. This result can be proved by previous research by Ghitas [30] where the pattern of spectral is increased within radiation intensity and remains constant in wavelength.

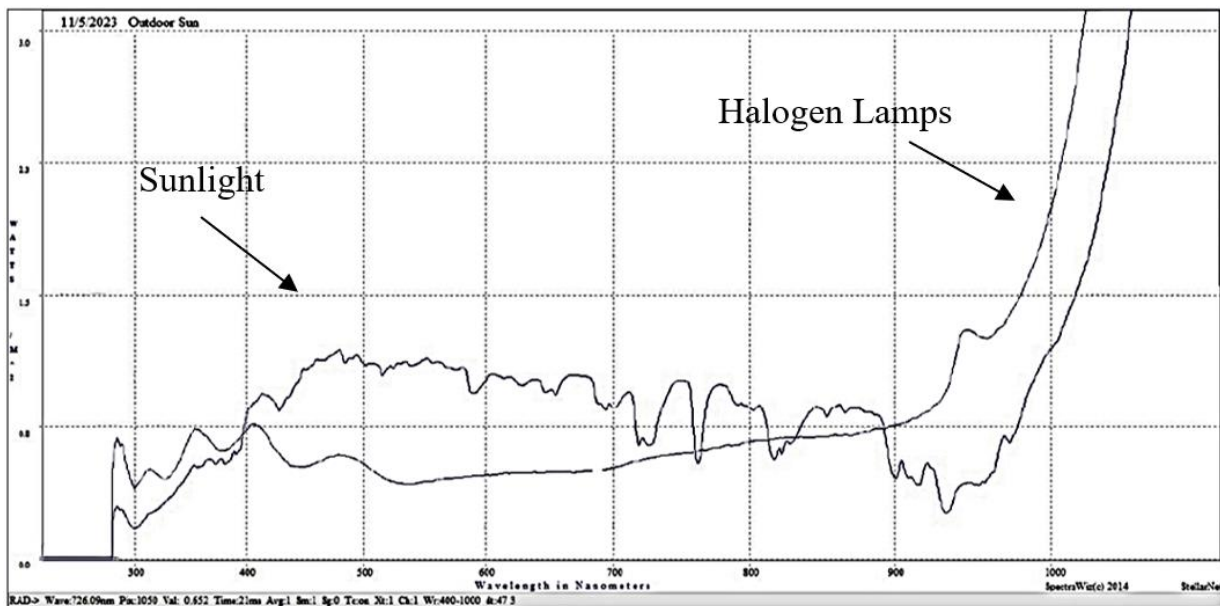


Fig. 5. Comparison of wavelength between sunlight and halogen lamps at 400W/m²

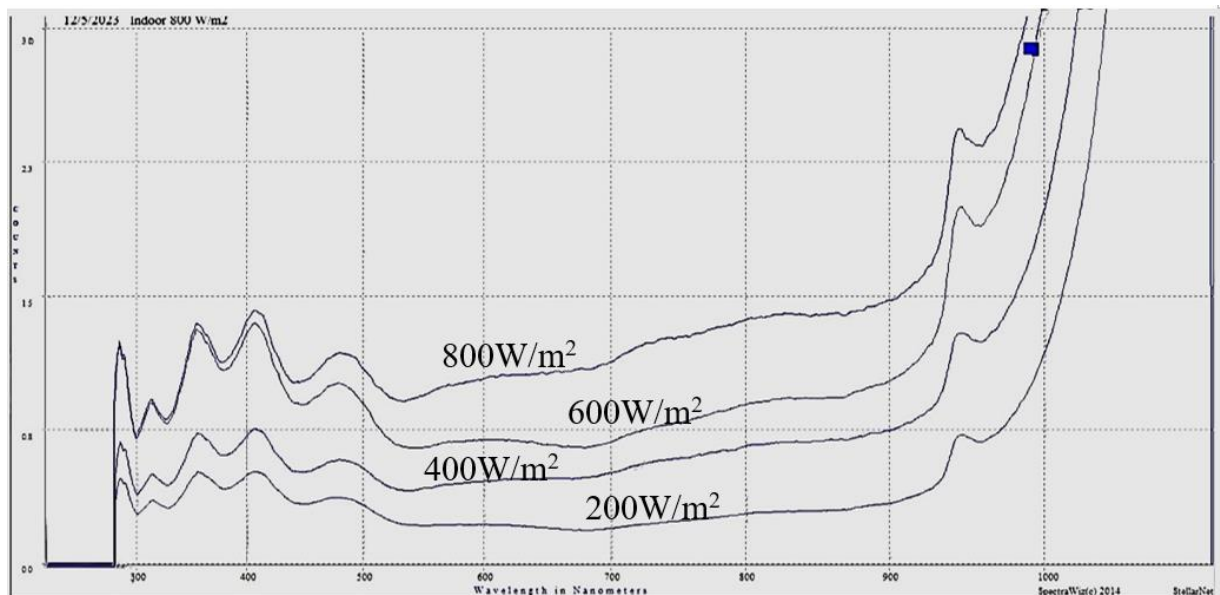


Fig. 6. Graph spectrum vs wavelength for indoor solar simulator

3.1.3 Temporal test

The results obtained from the temperature versus time graph in Figure 7 below indicate that the PV module takes approximately 40 minutes to reach a stable initial temperature, while the PV/T system takes around 54 minutes to cool down to initial temperature. This information is important as it provides the cooling characteristics of the PV and PV/T modules. It allows the planning of timing and duration of subsequent experiments, ensuring that the modules were at the stable desired ambient temperature before starting the next set of experiments to get a reliability result.

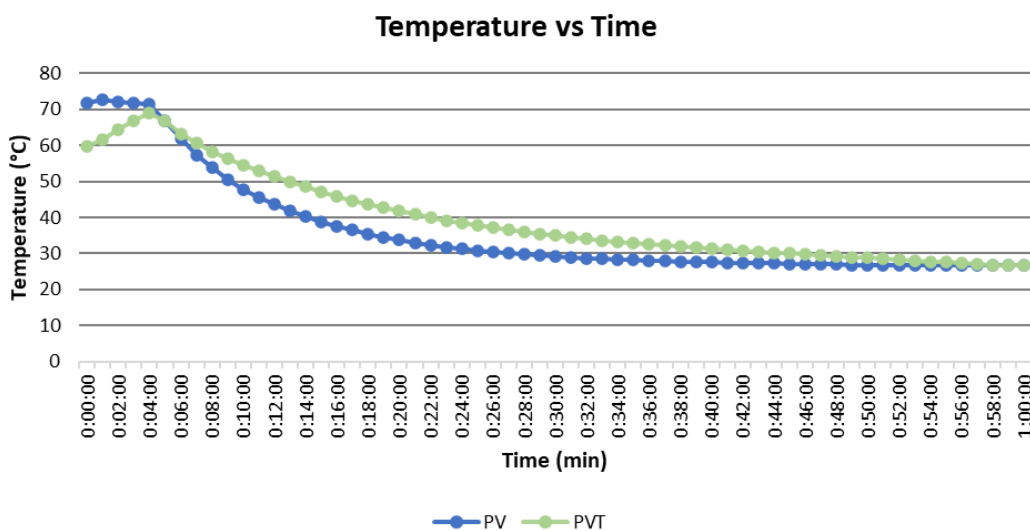


Fig. 7. Graph temperature vs time for temporal test

3.2 Characterization of Nanoparticles

Figure 8(a) shows the surface topography of MgO nanoparticles under magnification 25.0k. The high-resolution of FESEM image clearly shows the formation of nanoparticles, which the particles are spherical in size and uniform with relatively smooth surfaces. Some agglomeration of particles was observed, indicating a tendency for them to form clusters. Particles size of nano MgO observations were made at a higher magnification of 100k shown in Figure 8(b) and Figure 8(c). It was found that the particle size ranged between 65 to 200 nm.

As shown in Figure 9, the structural phase of MgO nanoparticles revealed that the diffraction peaks at $2\theta = 36.9792^\circ$, 42.96206° , 62.37967° , 74.78366° , and 78.731° are associated at (111), (200), (220), (311) and (222) crystallographic planes, respectively. which they can be constituted in a cubic phase of MgO according to JPCDS card no. 45-0946 at $2\theta = 37.02^\circ$, 43.02° , 58.72° , 76.78° , and 78.73° correspond to the plane (111), (200), (220), (311) and (222) [24,25]. No additional peaks were present in the XRD pattern indicated that the sample is highly pure, with no detectable impurities or additional phases. After calculating the particle size at each peak, the average particle size of the MgO sample was calculated to be 265.518 nm presented in Table 10.

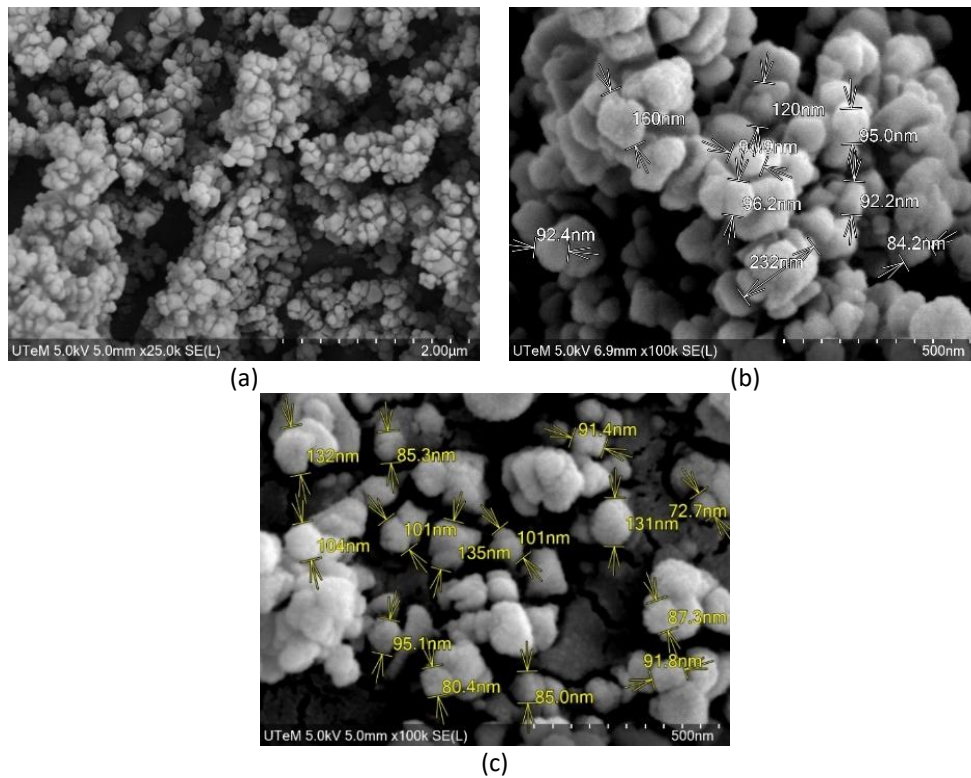


Fig. 8. (a) FESEM result under 25.0k magnification (b) Measurement of particles size at magnification 100k (c) Measurement of particles size under different angle

Table 10

XRD analysis data and particle size measurement

Max. 2θ	Crystallographic Plane	Intensity	FWHM	Particle Size (nm)
36.9792	(111)	145.60	0.26228	316.076
42.96206	(200)	155.05	0.29697	284.175
62.37967	(220)	99.90	0.40023	229.364
74.78366	(311)	84.45	0.43771	225.814
78.731	(222)	80.91	0.37322	272.159
Average particle size				265.518

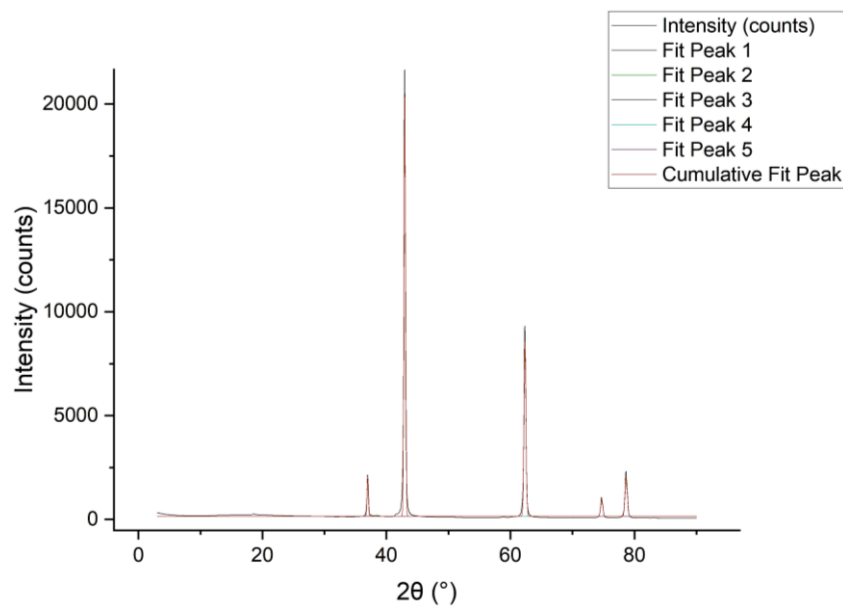


Fig. 9. XRD pattern of MgO nanoparticles

3.3 Stability of Nanofluids (Observation Method)

Table 11 summarizes the stability assessment of the nanofluid based on various concentrations of the nanoparticles MgO. The stability of the nanofluid was evaluated through visual observations of sedimentation and agglomeration. Table 12 shows the change of the mixed nanofluids in the period 14 days. The results obtained indicated that the 0.2% MgO concentration exhibited the highest stability among the five concentrations, with minimal sedimentation at the bottle's bottom. Conversely, the 1.0% MgO concentration displayed the lowest stability, marked by a thick sedimentation layer at the bottom of the bottle. In the present study, it was also observed that as the MgO concentration increased, the stability of the nanofluid dropped at nanofluid without surfactant. The higher the particle concentration, the poorer the stability of nanofluid [31,32]. Increase in particle concentration also increase particle cluster size due to lower interparticle distance and enhanced Van der Waal attractive force which directly affects the settling velocity [33].

Next, the sedimentation of nanofluid in present study may be caused by the nanoparticle size. Based on the Chakraborty and Panigrahi [33] claimed that the settling velocity of the nanoparticle is dependent on the size of particle. Low particle size and minimal density difference between nanoparticle and base fluid lead to lower settling velocity and therefore superior nanofluid stability [34]. The suggested size for nanofluid metal oxide is below 100nm [34]. In the present study, the average particle size is 265nm, which is much larger than the particle size done by previous researcher which range below 100nm. Also, the density of the nanoparticle MgO and distilled water is 3580kg/m³ and 997.1kg/m³ respectively which the density difference is quite high.




The surface coating of the nanoparticle or functionalization layers may also be one of the factors affected the overall stability of the nanofluid. As referred Roslan *et al.*, [35], the choice of surface coating is critical, as it can impact the stability of the nanofluid. the wrong or inadequate surface coating can lead to instability, such as particle agglomeration or phase separation. A good matching of the surface coating with the nanoparticles can improve the dispersion between nanoparticles with base fluid. Oppositely, the coating of the nanoparticles will cause the repulsive between base fluid and nanoparticles. In the present study, the specific coating on the MgO nanoparticles used in the nanofluid formulation was not characterized. However, the instability observed in some nanofluid samples may be attributed to the poor interactions between the coating layer and the base fluid. Incompatibility or weak interactions between the coating and the base fluid can lead to reduced stability, resulting in particle agglomeration or sedimentation.

Table 11

Level of stability of nanofluid in various concentration

MgO concentration (wt%)	Level of stability
0.2	Good
0.4	Moderate
0.6	Moderate
0.8	Moderate
1	Unstable

Table 12
 Stability observation of nanofluid in different period

Various Surfactant	1 day	7 days	14 days
Without Surfactant			

3.4 Thermophysical Properties of Nanofluids

3.4.1 Density

It was found that as the weight concentration increased, the density of the nanofluid also increased as shown in graph Figure 10. The result calculated had also validated as the line of present study in line with Ali *et al.*, [26]. This phenomenon can be explained by adding the nanoparticles which nanoparticles have higher density compared to base fluid led to a higher overall mass per unit volume resulting in an increase of the nanofluid density. Thus, the increased in the density improved the heat transfer characteristics of the nanofluid because the higher the fluid density the higher the thermal conductivity proved by Apmann *et al.*, [36].

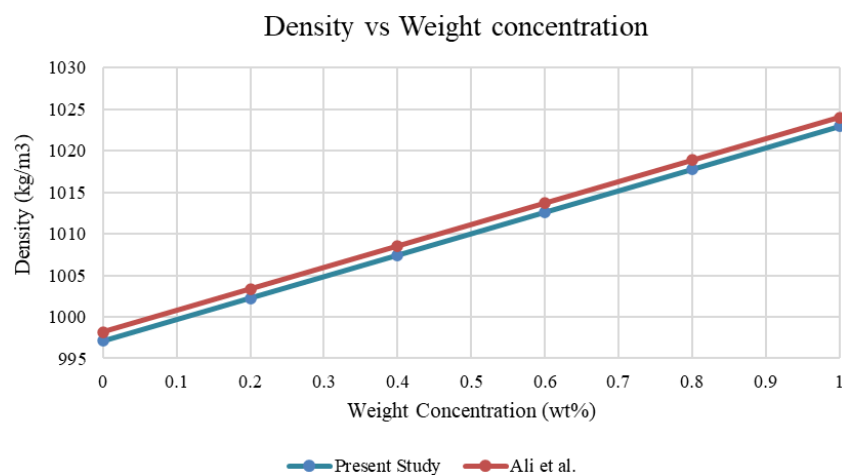


Fig. 10. Density versus weight concentration

3.4.2 Specific heat capacity

As shown in graph Figure 11, as the weight concentrations of the nanoparticles increased, the specific heat capacity of the nanofluid decreased. The line trend from the calculation is validated by Ali *et al.*, [26]. This happened due to nanoparticles have a lower specific heat capacity compared to the base fluid which is 903J/kg·K and 4184J/kg·K respectively. As the weight concentration of nanoparticles increased, their contribution to the overall specific heat capacity of the nanofluid became more significant, hence leading to a decrease in the specific heat capacity of the nanofluid.

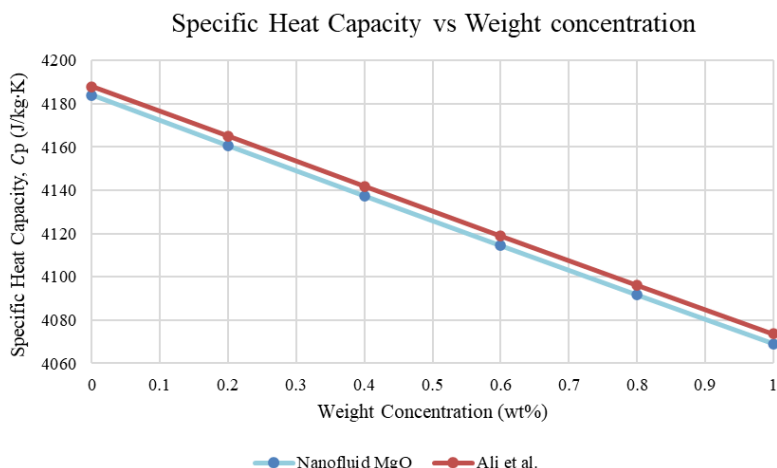


Fig. 11. Specific heat capacity versus weight concentration

3.4.3 Thermal conductivity

As shown in Figure 12, the result of thermal conductivity for MgO without surfactant revealed a positive correlation between weight concentration and thermal conductivity. The line trend from present study is validated by Verma *et al.*, [22]. As the concentration of MgO nanoparticles increased, the thermal conductivity of the nanofluid also increased. This can be attributed to the higher particle concentration, which leads to increased interactions between particles and enhanced thermal energy transfer within the nanofluid [11,21,22]. For Figure 13, it observed that as the temperature increased, the thermal conductivity of the nanofluid also increased. The line presented the same trend as Verma *et al.*, [22]. The increase in temperature increase in thermal conductivity behavior was due to the increased thermal energy and molecular vibrations at higher temperatures. As the temperature rises, the particles within the nanofluid experience more energetic collisions which enhance the overall thermal conductivity of the nanofluid [11,21,22].

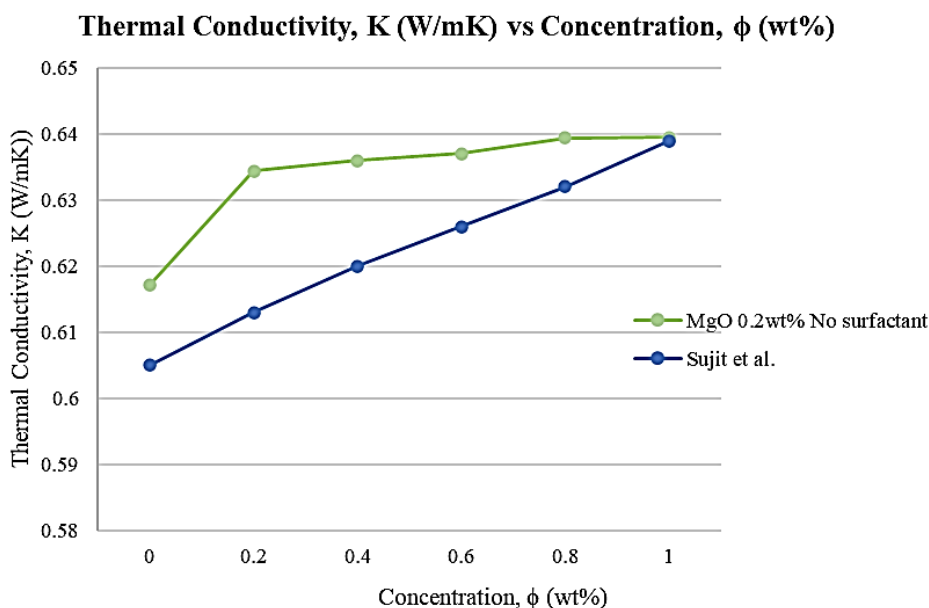


Fig. 12. Graph thermal conductivity versus concentration

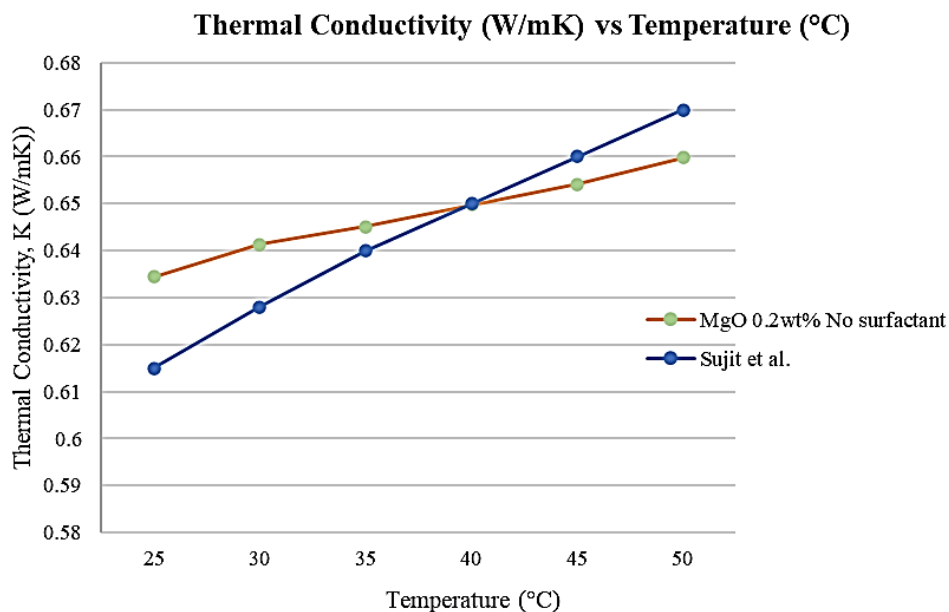


Fig. 13. Graph thermal conductivity versus temperature

3.4.4 Viscosity

As shown in Figure 14, the results obtained showed that as the concentration of the nanoparticles increased, the viscosity of the nanofluid increased. The line trend from present study is validated by Verma *et al.*, [22]. This is because as the MgO concentration rises, the interaction and collision between the nanoparticles also increases hence causing the increase of viscosity [11]. For Figure 15, it showed a negative trend which validated by Verma *et al.*, [22]., indicating that as the temperature increased, the viscosity of the nanofluid decreased. This is due to higher temperatures, the thermal energy causes the nanoparticles and base fluid molecules to move more freely, resulting in reduced intermolecular interactions and lower viscosity [11].

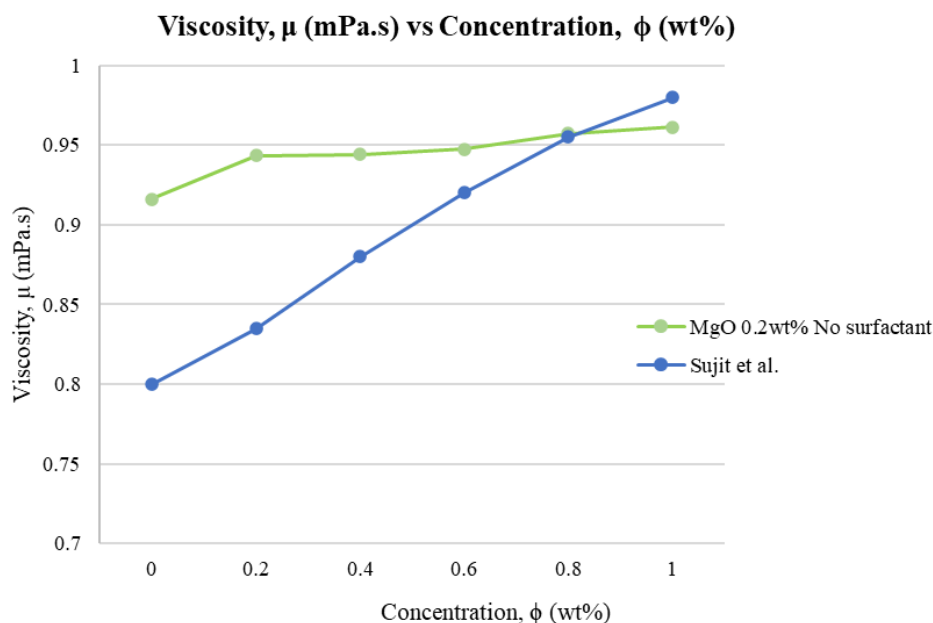


Fig. 14. Graph viscosity versus concentration

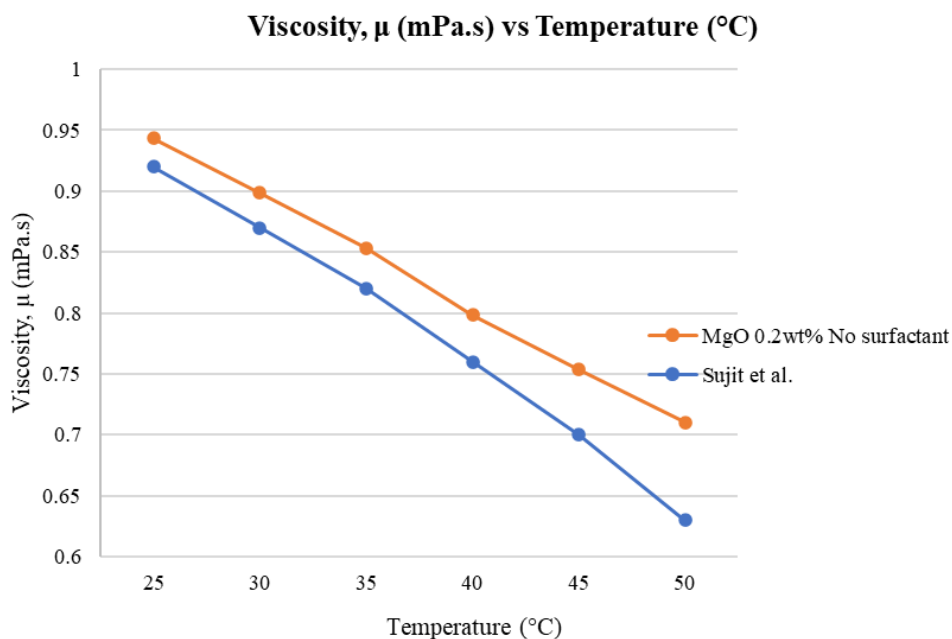


Fig. 15. Graph viscosity versus temperature

3.5 Measurement of Efficiency

3.5.1 Thermal efficiency

A bar chart analysis in Figure 16 showed that as the irradiance increased, the thermal efficiency of the system decreased. In the case of using water as the working fluid, an increase in flow rate was found to correspond with an increase in thermal efficiency. This can be explained by considering that higher flow rates allow for better heat transfer and reduced residence time, minimizing heat losses and improving overall system efficiency. Meanwhile, the thermal efficiency of the nanofluid exhibited a different trend with flow rate whereas the flow rate increased, the thermal efficiency of the nanofluid decreased. This was due to the optimum flow rate of the nanofluid was below 10L/h which is not determined yet because it is not within the study scope range which is 10L/h, 20L/h and 30L/h in the present study. This can be proved by previous research Verma *et al.*, [22] where the relationship between the thermal efficiency and flow rate is not straightforward, increasing the flow rate of the working fluid resulted in an improvement in thermal efficiency. However, beyond a certain optimum flow rate, further increases in flow rate led to a decline in thermal efficiency. The result obtained in the present study was located at the decline trend which indicated that the flow rate 10L/h, 20L/h and 30L/h exceeded the optimum flow rate for nanofluid. The efficiency of a PV/T system can be significantly influenced by various design parameters, including the diameter and length of the serpentine tubes, as well as the choice of materials [21,37,38]. These factors collectively impact the system's overall performance, particularly the optimal flow rate required to achieve peak efficiency. It's important to acknowledge that distinct PV/T system designs will inherently possess unique configurations, leading to varying optimum flow rates necessary for attaining maximum efficiency [37,38].

Due to the concern, a flow rate of 10 L/h was selected as a benchmark for the ease of the comparison between two working fluids. As compared water and nanofluid in 10L/h, it was observed that nanofluid had the highest 74% of thermal efficiency increment compared to the water at 500W/m² followed by 71% at 200w/m² and 55% at 800W/m². As referred to Figure 17, at 10L/h of flow rate, the PV/T surface temperature for nanofluid as working temperature were slightly lower compared water as working fluid where 1.61 $^{\circ}$ C for 500W/m², 1.27 $^{\circ}$ C for 800W/m² and 0.84 $^{\circ}$ C for

200W/m². Although the exact optimal flow rate for the nanofluid was not determined in this study, the result obtained evidenced that the nanofluid exhibits higher thermal efficiency compared to water at 10 L/h under varying irradiance levels. This comparison had highlighted the superior performance of the nanofluid in terms of thermal efficiency when compared to water. The nanofluid's ability to enhance heat transfer and improve overall system efficiency at a flow rate of 10L/h demonstrates its potential for application in PV/T system.

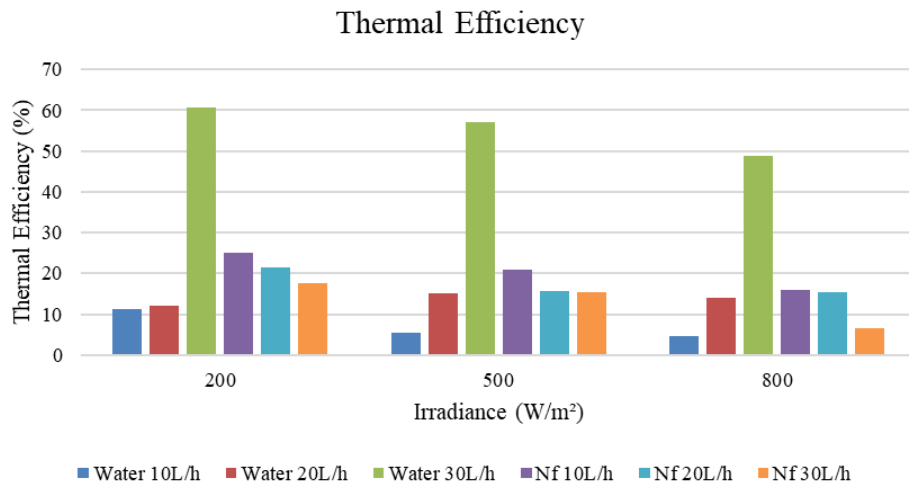


Fig. 16. Thermal efficiency for various flow rate of water and nanofluid in various irradiance intensities

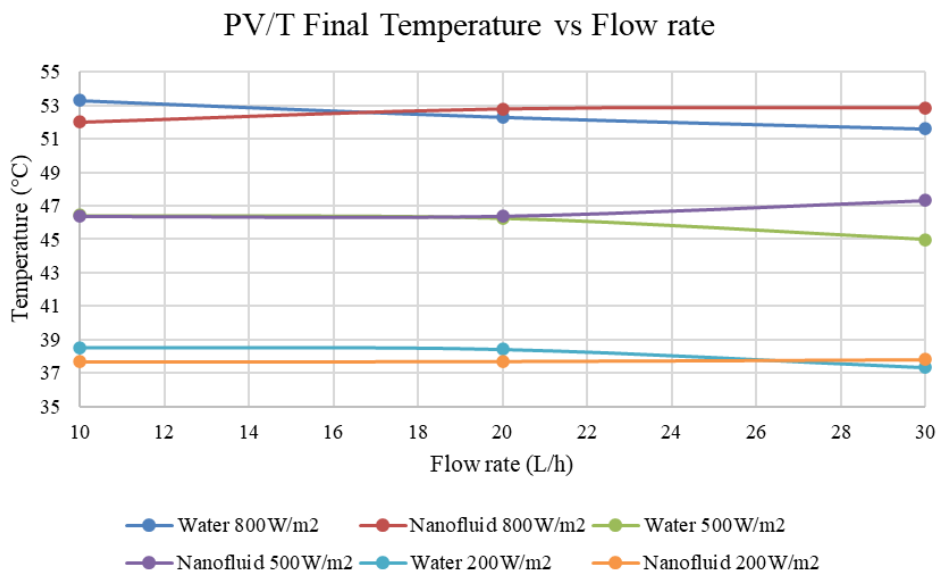


Fig. 17. Graph final temperature PV/T versus flow rate at different irradiance

3.5.2 Electrical efficiency

The result in Figure 18 showed that as the flow rate increased, the electrical efficiency for water as working fluid increased, while for nanofluid, it presented an opposite trend compared with the water. This phenomenon is related to the previous section 3.4.1 where the thermal efficiency had a close interconnected to the electrical efficiency. The experimental results demonstrated a clear correlation between the thermal efficiency and electrical efficiency. As the thermal efficiency of the system improved, there was a corresponding increase in the electrical efficiency. This can be attributed to the fact that a higher thermal efficiency reduces the PV/T surface temperature,

resulting in a lower operating temperature for the PV module [20]. The lower temperature enhances the electrical performance of the PV cells, leading to an overall increase in electrical efficiency [12,20,27].

The electrical efficiency of the PV/T system was further analyzed in comparison between nanofluid and water at flow rate 10L/h. Nanofluid demonstrated a 5% increase in electrical efficiency at 200W/m², 2.1% increase at 500W/m², and 1.9% increase at 800W/m², compared to water. These findings indicate that the incorporation of nanoparticles in the nanofluid formulation positively influences the electrical efficiency of the PV/T system. The experimental results also revealed that nanofluid 10L/h exhibited the highest electrical efficiency among all the flow rates. This suggests that the nanofluid has the ability to absorb heat not only at the PV/T surface but also throughout the system. By effectively absorbing and distributing heat, the nanofluid enables a more efficient conversion of solar energy into electrical power, leading to higher electrical efficiency compared to water.

The relationship between electrical efficiency and the I-V curve in different solar irradiances was also examined as shown in Figure 19(a), (b) and (c). It was observed that as the electrical efficiency increased, the voltage output of the PV module also increased while the current output remains constant due to the constant irradiance level during the experiments. With a higher electrical efficiency, more of the incident solar energy is effectively converted into electrical power, resulting in an increased voltage output [11,20]. When compared with the voltage PV, PV/T-water and PV/T-nanofluid at 10L/h, PV/T nanofluid had an increment 2.7% of voltage compared to PV and 1.4% to PV/T-water at 800W/m². While at 500w/m², PV/T-nanofluid achieved a 2.3% increment of voltage compared to PV and 1.3% to PV/T-water and 1.7% and 1% increased for PV and PV/T-water respectively at 200W/m². Which means the higher the voltage, the higher the power output produced.

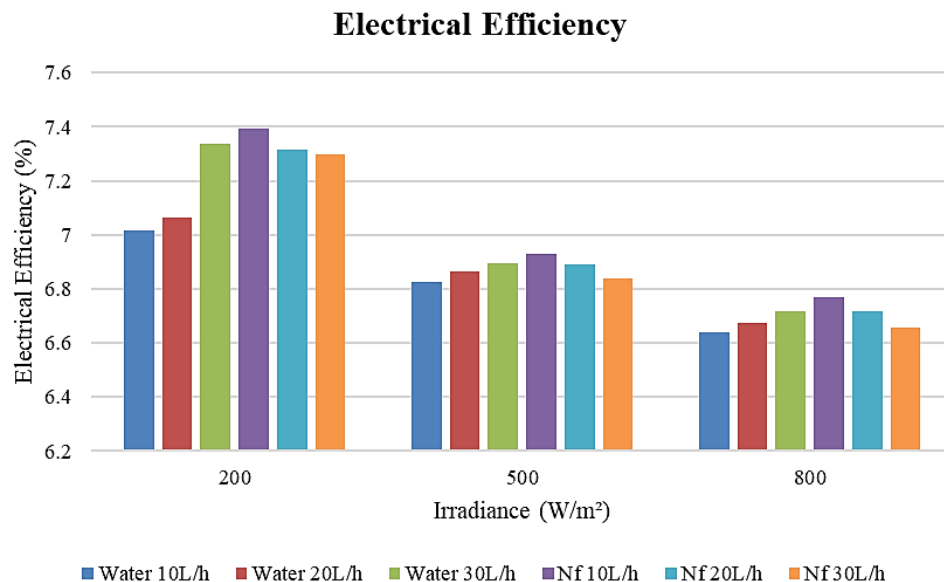


Fig. 18. Electrical efficiency for various flow rate of water and nanofluid in various irradiance intensities

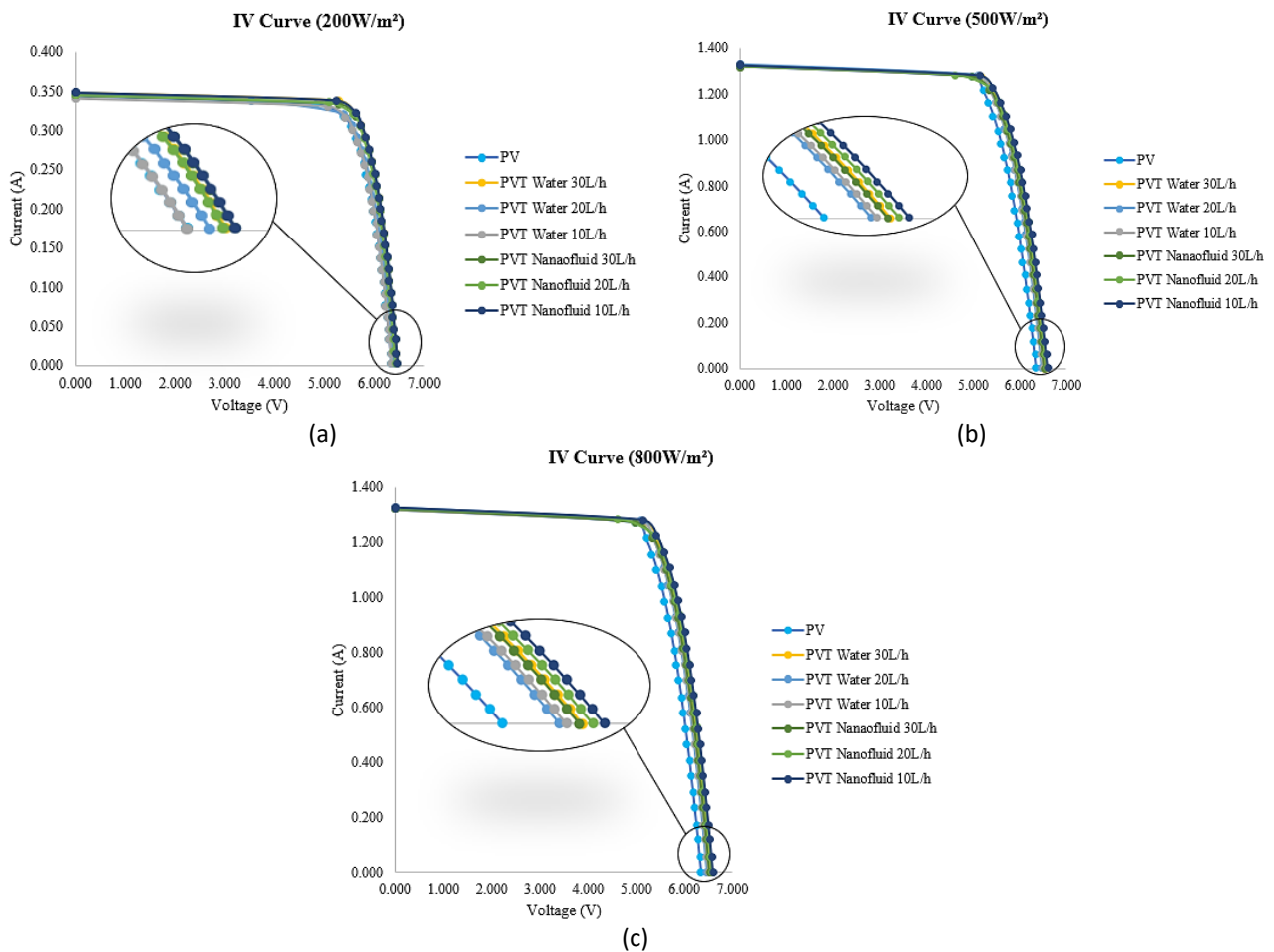


Fig. 19. I-V curve for (a) 200W/m² (b) 500W/m² (c) 800W/m²

3.5.3 Overall efficiency

The overall efficiency of the PV/T system was evaluated by considering both the thermal efficiency and electrical efficiency. The results in Figure 20 demonstrated that water 30L/h exhibited higher overall efficiency, but based on aforementioned, the nanofluid optimum flow rate was not determined due to the optimum flow rate of the nanofluid was not fall in the range of study scope. indicating its potential for improved energy conversion and utilization. As discussed earlier, nanofluid at 10L/h flow rate exhibited higher thermal efficiency and electrical efficiency compared to water. The combination of these enhanced efficiencies contributed to the higher overall efficiency of the nanofluid-based PV/T system. By effectively absorbing and transferring heat, the nanofluid improved the thermal performance of the system, reducing heat losses and optimizing heat utilization. The increased electrical efficiency of the nanofluid allowed for a more efficient conversion of solar energy into electrical power. This improved electrical efficiency correlated with the high thermal efficiency, contributed to the higher overall efficiency observed in the nanofluid based PV/T system.

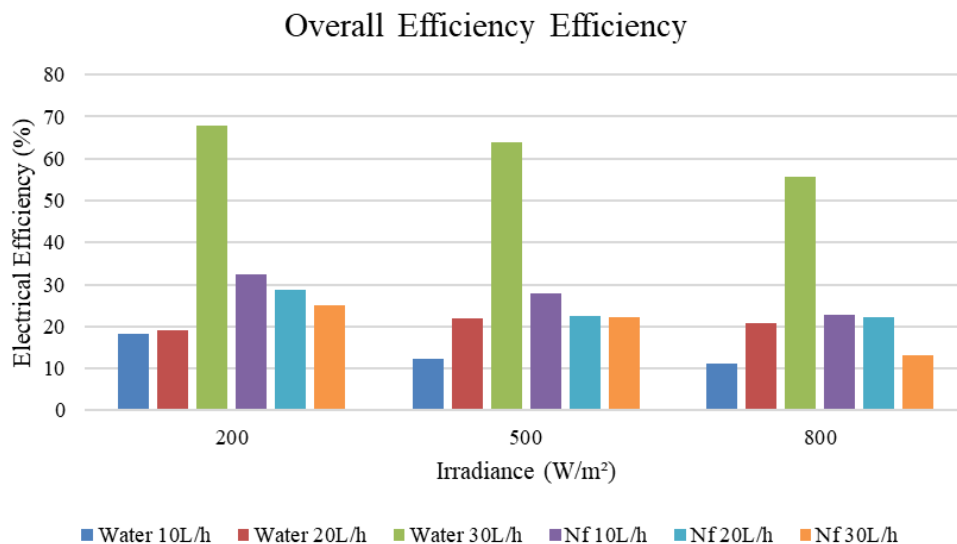


Fig. 20. Overall efficiency for various flow rate of water and nanofluid in various irradiance intensities

4. Conclusions

This study analysed the PV/T efficiency based on variations of irradiances and flow rates, using nanofluid MgO and water as the working fluid. From our analysis, we drew several conclusions discussed in the following:

- i. MgO nanofluids with a concentration of 0.2% without surfactant demonstrated the highest level of stability which did not show any significant sedimentation and agglomeration more than 14 days among all the mixtures tested
- ii. Increasing the concentration of nanoparticles enhances the thermal conductivity of the nanofluid, while higher temperatures also contribute to increased thermal conductivity. With an increase in nanoparticle concentration, the viscosity of the nanofluid increased, while rising temperatures resulted in a decrease in nanofluid viscosity.
- iii. Optimum flow rate was not in the range of scope study. However, at flow rate 10L/h, nanofluid demonstrated a 5% increase in electrical efficiency at 200W/m², 2.1% increase at 500W/m², and 1.9% increase at 800W/m², compared to water. Also, nanofluid had the highest 74% of thermal efficiency increment compared to the water at 500W/m² followed by 71% at 200w/m² and 55% at 800W/m²

Acknowledgement

The author would like to thank Fakulti Kejuruteraan Mekanikal, Universiti Teknikal Malaysia Melaka Applied Solar Energy Laboratory, FKM Chemical Laboratory to support the project.

References

- [1] Gupta, Sanjeev Kumar, Harshita Verma, and Neha Yadav. "A review on recent development of nanofluid utilization in shell & tube heat exchanger for saving of energy." *Materials Today: Proceedings* 54 (2022): 579-589. <https://doi.org/10.1016/j.matpr.2021.09.455>
- [2] Gupta, Sanjeev Kumar Gupta, and Abhishek Saxena. "A progressive review of hybrid nanofluid utilization in solar parabolic trough collector." *Materials Today: Proceedings* (2023). <https://doi.org/10.1016/j.matpr.2023.06.204>
- [3] Li, Danny HW, Liu Yang, and Joseph C. Lam. "Zero energy buildings and sustainable development implications-A review." *Energy* 54 (2013): 1-10. <https://doi.org/10.1016/j.energy.2013.01.070>

- [4] Rosli, M. A. M., S. Misha, K. Sopian, S. Mat, M. Yusof Sulaiman, and E. Salleh. "Parametric analysis on heat removal factor for a flat plate solar collector of serpentine tube." *World Applied Sciences Journal* 29, no. 2 (2014): 184-187.
- [5] Soltani, Shohreh, Alibakhsh Kasaeian, Hamid Sarrafha, and Dongsheng Wen. "An experimental investigation of a hybrid photovoltaic/thermoelectric system with nanofluid application." *Solar Energy* 155 (2017): 1033-1043. <https://doi.org/10.1016/j.solener.2017.06.069>
- [6] Rosli, Mohd Afzanizam Mohd, Danial Shafiq Mohd Zaki, Fatiha Abdul Rahman, Suhaila Sepeai, Nurfaizey Abdul Hamid, and Muhammad Zaid Nawam. "F-chart method for design domestic hot water heating system in Ayer Keroh Melaka." *Journal of Advanced Research in Fluid Mechanics and Thermal Sciences* 56, no. 1 (2019): 59-67.
- [7] Chowdhury, Sumon, and Md Razon Chowdhury. "Advancements of air, water and nanofluid based photovoltaic thermal (PV/T) technologies." In *2017 2nd International Conference on Electrical & Electronic Engineering (ICEEE)*, pp. 1-4. IEEE, 2017. <https://doi.org/10.1109/ICEEE.2017.8412852>
- [8] Sachit, F. A., Noreffendy Tamaldin, M. A. M. Rosli, S. Misha, and A. L. Abdullah. "Current progress on flat-plate water collector design in photovoltaic thermal (PV/T) systems: A Review." *Journal of Advanced Research in Dynamical and Control Systems* 10, no. 4 (2018): 680-89.
- [9] Wu, Shuang-Ying, Qiao-Ling Zhang, Lan Xiao, and Feng-Hua Guo. "A heat pipe photovoltaic/thermal (PV/T) hybrid system and its performance evaluation." *Energy and Buildings* 43, no. 12 (2011): 3558-3567. <https://doi.org/10.1016/j.enbuild.2011.09.017>
- [10] Bin Mohd Rosli, Mohamad Afzanizam, Sohif Mat, Kamaruzzaman Sopian, Mohd Yusof Sulaiman, Elias Ilias Salleh, and Mohd Khairul Anuar Sharif. "Thermal performance on unglazed photovoltaic thermal polymer collector." *Advanced Materials Research* 911 (2014): 238-242. <https://doi.org/10.4028/www.scientific.net/AMR.911.238>
- [11] Al-Waeli, Ali HA, Miqdam T. Chaichan, Hussein A. Kazem, and Kamaruzzaman Sopian. "Comparative study to use nano-(Al₂O₃, CuO, and SiC) with water to enhance photovoltaic thermal PV/T collectors." *Energy Conversion and Management* 148 (2017): 963-973. <https://doi.org/10.1016/j.enconman.2017.06.072>
- [12] Gupta, Sanjeev Kumar, Shubham Gupta, and Rajeev Singh. "A comprehensive review of energy saving in shell & tube heat exchanger by utilization of nanofluids." *Materials Today: Proceedings* 50 (2022): 1818-1826. <https://doi.org/10.1016/j.matpr.2021.09.212>
- [13] Salem Ahmed, Mahmoud. "Nanofluid: New Fluids by Nanotechnology." *Thermophysical Properties of Complex Materials* (2019). <https://doi.org/10.5772/intechopen.86784>
- [14] Rosli, Mohd Afzanizam Mohd, Yew Wai Loon, Muhammad Zaid Nawam, Suhaimi Misha, Aiman Roslizar, Faridah Hussain, Nurfaizey Abdul Hamid, Zainal Arifin, and Safarudin Gazali Herawan. "Validation Study of Photovoltaic Thermal Nanofluid Based Coolant Using Computational Fluid Dynamics Approach." *CFD Letters* 13, no. 3 (2021): 58-71. <https://doi.org/10.37934/cfdl.13.3.5871>
- [15] Al-Ghezi, Moafaq KS, Khaleel I. Abass, Ahmed Q. Salam, Raid S. Jawad, and Hussein A. Kazem. "The possibilities of using nano-CuO as coolants for PVT system: An experimental study." In *Journal of Physics: Conference Series*, vol. 1973, no. 1, p. 012123. IOP Publishing, 2021. <https://doi.org/10.1088/1742-6596/1973/1/012123>
- [16] Sardarabadi, Mohammad, Mohammad Passandideh-Fard, and Saeed Zeinali Heris. "Experimental investigation of the effects of silica/water nanofluid on PV/T (photovoltaic thermal units)." *Energy* 66 (2014): 264-272. <https://doi.org/10.1016/j.energy.2014.01.102>
- [17] Khan, Ajiv Alam, Mohd Danish, Saeed Rubaiee, and Syed Mohd Yahya. "Insight into the investigation of Fe₃O₄/SiO₂ nanoparticles suspended aqueous nanofluids in hybrid photovoltaic/thermal system." *Cleaner Engineering and Technology* 11 (2022): 100572. <https://doi.org/10.1016/j.clet.2022.100572>
- [18] Hussien, Hashim A., M. Hasanuzzaman, Ali H. Noman, and Abdulmunem R. Abdulmunem. "Enhance photovoltaic/thermal system performance by using nanofluid." In *3rd IET International Conference on Clean Energy and Technology (CEAT)* 2014, pp. 1-5. IET, 2014. <https://doi.org/10.1049/cp.2014.1515>
- [19] Ghadiri, Matin, Mohammad Sardarabadi, Mohammad Pasandideh-fard, and Ali Jabari Moghadam. "Experimental investigation of a PVT system performance using nano ferrofluids." *Energy Conversion and Management* 103 (2015): 468-476. <https://doi.org/10.1016/j.enconman.2015.06.077>
- [20] Hasan, Husam Abdurassool, Kamaruzzaman Sopian, Ahed Hameed Jaz, and Ali Najah Al-Shamani. "Experimental investigation of jet array nanofluids impingement in photovoltaic/thermal collector." *Solar Energy* 144 (2017): 321-334. <https://doi.org/10.1016/j.solener.2017.01.036>
- [21] Choudhary, Suraj, Anish Sachdeva, and Pramod Kumar. "Investigation of the stability of MgO nanofluid and its effect on the thermal performance of flat plate solar collector." *Renewable Energy* 147 (2020): 1801-1814. <https://doi.org/10.1016/j.renene.2019.09.126>
- [22] Verma, Sujit Kumar, Arun Kumar Tiwari, and Durg Singh Chauhan. "Performance augmentation in flat plate solar collector using MgO/water nanofluid." *Energy Conversion and Management* 124 (2016): 607-617. <https://doi.org/10.1016/j.enconman.2016.07.007>

- [23] Cui, Yun, and Qunzhi Zhu. "Study of photovoltaic/thermal systems with MgO-water nanofluids flowing over silicon solar cells." In *2012 Asia-Pacific Power and Energy Engineering Conference*, pp. 1-4. IEEE, 2012. <https://doi.org/10.1109/APPEEC.2012.6307203>
- [24] Bdewi, Shahbaa F., Ayad M. Abdulrazaka, and Bakhtyar K. Aziz. "Catalytic Photodegradation of Methyl orange using MgO nanoparticles prepared by molten salt method." *Asian Transactions on Engineering* 5, no. 6 (2015): 1-5.
- [25] Salman, Khansaa D., Haider H. Abbas, and Hussain A. Aljawad. "Synthesis and characterization of MgO nanoparticle via microwave and sol-gel methods." In *Journal of Physics: Conference Series*, vol. 1973, no. 1, p. 012104. IOP Publishing, 2021. <https://doi.org/10.1088/1742-6596/1973/1/012104>
- [26] Ali, Abdallah Yousef Mohammed, Ahmed Hassan El Shazly, Marwa Farouk El-Kady, Hesham Ibrahim Elqady, Kholoud Madih, and Essam Hares. "Experimental and Theoretical Studies of Thermophysical Properties of MgO-Water Nanofluid." In *Materials Science Forum*, vol. 1008, pp. 47-52. Trans Tech Publications Ltd, 2020. <https://doi.org/10.4028/www.scientific.net/MSF.1008.47>
- [27] Sundar, Lingala Syam, Solomon Mesfin, Zafar Said, Manoj K. Singh, V. Punnaiah, and António CM Sousa. "Energy, economic, environmental and heat transfer analysis of a solar flat-plate collector with pH-treated Fe₃O₄/water nanofluid." *International Journal of Energy for a Clean Environment* 22, no. 6 (2021). <https://doi.org/10.1615/InterJEnerCleanEnv.2021036464>
- [28] Sundar, L. Syam, and Kotturu VV Chandra Mouli. "Experimental analysis and Levenberg-Marquardt artificial neural network predictions of heat transfer, friction factor, and efficiency of thermosyphon flat plate collector with MgO/water nanofluids." *International Journal of Thermal Sciences* 194 (2023): 108555. <https://doi.org/10.1016/j.ijthermalsci.2023.108555>
- [29] Ali, Abu Raihan Ibna, and Bodius Salam. "A review on nanofluid: preparation, stability, thermophysical properties, heat transfer characteristics and application." *SN Applied Sciences* 2, no. 10 (2020): 1636. <https://doi.org/10.1007/s42452-020-03427-1>
- [30] Ghitas, Ahmed Elsayed. "Studying the effect of spectral variations intensity of the incident solar radiation on the Si solar cells performance." *NRIAG Journal of Astronomy and Geophysics* 1, no. 2 (2012): 165-171. <https://doi.org/10.1016/j.nrjag.2012.12.013>
- [31] Chakraborty, Samarshi, Ishita Sarkar, Krishnayan Haldar, Surjya Kanta Pal, and Sudipto Chakraborty. "Synthesis of Cu-Al layered double hydroxide nanofluid and characterization of its thermal properties." *Applied Clay Science* 107 (2015): 98-108. <https://doi.org/10.1016/j.clay.2015.01.009>
- [32] Chakraborty, Samarshi, Ishita Sarkar, Avinash Ashok, Iman Sengupta, Surjya K. Pal, and Sudipto Chakraborty. "Thermo-physical properties of Cu-Zn-Al LDH nanofluid and its application in spray cooling." *Applied Thermal Engineering* 141 (2018): 339-351. <https://doi.org/10.1016/j.applthermaleng.2018.05.114>
- [33] Chakraborty, Samarshi, and Pradipta Kumar Panigrahi. "Stability of nanofluid: A review." *Applied Thermal Engineering* 174 (2020): 115259. <https://doi.org/10.1016/j.applthermaleng.2020.115259>
- [34] Yu, Fan, Yingying Chen, Xingbo Liang, Jiale Xu, Chiahsun Lee, Qi Liang, Peng Tao, and Tao Deng. "Dispersion stability of thermal nanofluids." *Progress in natural science: Materials International* 27, no. 5 (2017): 531-542. <https://doi.org/10.1016/j.pnsc.2017.08.010>
- [35] Roslan, Anis Arisa, Siti Nur Azella Zaine, Hasnah Mohd Zaid, Mursyidah Umar, and Hoe Guan Beh. "Nanofluids stability on amino-silane and polymers coating titanium dioxide and zinc oxide nanoparticles." *Engineering Science and Technology, an International Journal* 37 (2023): 101318. <https://doi.org/10.1016/j.jestch.2022.101318>
- [36] Apmann, Kevin, Ryan Fulmer, Alberto Soto, and Saeid Vafaei. "Thermal conductivity and viscosity: Review and optimization of effects of nanoparticles." *Materials* 14, no. 5 (2021): 1291. <https://doi.org/10.3390/ma14051291>
- [37] Moravej, Mojtaba, Mehdi Vahabzadeh Bozorg, Yu Guan, Larry KB Li, Mohammad Hossein Doranehgard, Kun Hong, and Qingang Xiong. "Enhancing the efficiency of a symmetric flat-plate solar collector via the use of rutile TiO₂-water nanofluids." *Sustainable Energy Technologies and Assessments* 40 (2020): 100783. <https://doi.org/10.1016/j.seta.2020.100783>
- [38] Kang, Woobin, Yunchan Shin, and Honghyun Cho. "Economic analysis of flat-plate and U-tube solar collectors using an Al₂O₃ nanofluid." *Energies* 10, no. 11 (2017): 1911. <https://doi.org/10.3390/en10111911>